J. Am. Ceram. Soc., 71 [6] 465-72 (1988)

Near-Tip Mechanics of Stress-Induced Microcracking in Brittle Materials

PANAYIOTIS G. CHARALAMBIDES and ROBERT M. McMEEKING

Department of Materials and Department of Mechanical Engineering, University of California, Santa Barbara, California 93106

A continuum-mechanics description of stress-induced microcracking was developed. Modulus-reduction effects due to microcracking are taken into account through the model of Budiansky and O'Connell. This is used in conjunction with a modified microcracking criterion that stems from the work of Evans and Fu. The resulting constitutive law for a microcracking material was used in finite-element calculations to study the near-tip stress and strain fields and the size and shape of a small-scale damaged zone for a stationary mode I crack in an elastic body. The finite-element results for the stationary crack are used to predict asymptotic toughening values which correspond to a fully developed wake of microcracked material for a propagating crack. Substantial toughening can result. In contrast, the microcracking zone for a stationary crack is thought to make little or no contribution to material toughening. The theoretical results are discussed in the context of experimental observations for zirconia-toughened alumina.

I. Introduction

Evidence suggests that microcracking accompanies crack propagation in some ceramics. Much of the evidence is indirect, but in the case of zirconia-toughened alumina (ZTA) which derives some of its enhanced toughness from stress-induced phase transformations, the creation of microcracks in the tip field of a growing crack was observed by means of electron microscopy.[1,2] In other materials, microcracks were not observed directly. However, evidence of grain-boundary movements and increased permeability adjacent to fracture surfaces of rock,[3] acoustic emission during crack growth in rock,[4] acoustic emission in porcelain,[5] rising toughness during crack growth in hafnium titanate[6] and in alumina,[7] and loss of toughness following removal of material adjacent to a propagated crack in alumina[8] can be interpreted as indicating the creation of microcracks by a propagating crack. On the other hand, all of the indirect evidence can be interpreted otherwise. Indeed, Swanson *et al.*[9] presented convincing evidence that some, if not all, of the increased toughness of coarse-grained alumina after crack gowth results from unbroken particles bridging and constraining the opening of the fracture trace. Thus, the likelihood that microcracks toughen coarse-grained alumina is doubted, and, at the same time, the bridging mechanism is known to operate in rocks and concrete.[9]

The direct observations in ZTA, however, indicate clearly that microcracks form in the crack field.[1] Furthermore, the applied-stress-induced microcracks in that case occur around monoclinic-zirconia particles which were thermally transformed from the tetragonal state before the crack-growth experiments were performed.[2] The toughness of this material containing mostly monoclinic zirconia is comparable to ZTA containing mostly tetragonal zirconia.[1] Thus, it is unlikely that the toughness of the ZTA containing mostly monoclinic zirconia can be attributed entirely to stress-induced phase transformations (tetragonal to monoclinic) without microcracking playing some role. It is possible that when near-crack-tip microcracking occurs, it influences the toughening by altering the extent around the crack of stress-induced phase transformation of the tetragonal zirconia present in the microstructure of the ZTA. However, the possibility must be considered that microcracking makes a direct contribution to toughening independent of any simultaneous phase transformations.

A purely theoretical model for microcrack toughening in brittle materials is presented here. Several such models were developed.[10-18] Some models[10-12,16] consider the nucleation and influence of discrete microcracks near a crack tip, whereas the rest use a continuum phenomenology to account for the creation and effects of such flaws. As such they are damage theories[19-21] for the material behavior. The model presented in the present paper uses such a continuum-damage theory for microcracking and is substantially based on the approach of Evans and Fu.[15] They developed their model for single-phase ceramics thought to microcrack on grain boundaries subjected to applied stress and residual stress due to thermal-expansion anisotropy.[22,23] However, we slightly modified the Evans and Fu model for the creation of microcracks due to applied stress to allow a simple multi-axial generalization. In addition, the present paper allows for the effect of microcracks on the elastic compliance but omits the dilatation associated with the relief of residual tensile stress. The concept used by Evans and Fu[15] of a saturation density of microcracks is retained, and, thus, above a certain stress the elastic modulus becomes insensitive to the strain but with a lower value than for the unmicrocracked material. Since there is no inclusion of the effects of residual stress relieved by microcracks, the material always unloads to zero strain when the stress is removed. Where the present paper goes beyond Evans and Fu[15] is that the boundary-value problems involved for stationary cracks are solved approximately by the finite-element method. Consequently, the results for the size and shape of microcrack zones at the crack tip and for distributions of stress, strain, and microcracks within that zone are more reliable.

Thereafter, the distribution of microcracks left in a wake by a propagating crack is deduced by use of a model in which the material is convected through the computed stationary zone. This allows an estimation of the toughening effect due to the compliance change of the material in such a wake.

In view of the foregoing, the work described in the present paper should be viewed as a purely theoretical treatment of an idealized model for the effect of microcracking. The results are useful for judging the potency of the hypothetical toughening associated with compliance increase due to microcracking if generated by a propagating crack.

II. The Microcracking Criterion and Constitutive Law

The hypothetical microcracking behavior used in the present paper is one in which the density of microcracks increases linearly with applied stress. We use ε as the isotropic microcrack density as defined by Budiansky and O'Connell[24] to be proportional to the number of microcracks per unit volume times an effective volume for the microcracks. When there are N circular microcracks per unit volume and the flaws have a radius $\ell/2$, then $\varepsilon = N\ell^3/8$ where ℓ is the grain-boundary-facet diameter. The microcracking criterion used is such that for monotonically increasing stress

$$\varepsilon = 0 \qquad (\text{for } \sigma_e < \sigma_c) \tag{1a}$$

$$\varepsilon = \lambda(\sigma_e - \sigma_c) \qquad (\text{for } \sigma_c \le \sigma_e \le \sigma_m) \tag{1b}$$

$$\varepsilon = \varepsilon_s = \lambda(\sigma_m - \sigma_c) \qquad (\text{for } \sigma_e > \sigma_m) \tag{1c}$$

Manuscript No. 199728. Received June 27, 1986; approved December 8, 1987. Supported by the U.S. Department of Energy through a contract with the Materials Research Laboratory at the University of Illinois at Champaign-Urbana.

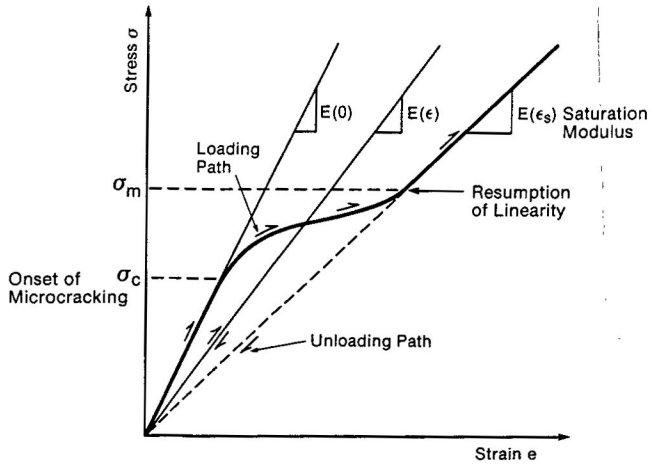

Fig. 1. Stress–strain curve for a microcracking material.

and ε cannot decrease. The quantity $\sigma_e = \sqrt{\sigma_{ij}\sigma_{ij}}$ is an effective applied stress, σ_c is the threshold stress for the initiation of microcracking, λ is the rate of increase of the microcrack density with stress, and σ_m is the effective stress at which microcracking ceases. The cessation of microcracking gives rise to a saturation density of microcracks ε_s. We take σ_c, λ, and ε_s to be material constants. Equations (1*a*) through (1*c*) are similar to the law of Fu and Evans[22,23] except that their parameter equivalent to λ mildly depends on the stress state. The magnitude of σ_c will depend on the ease with which microcrack nuclei fail and the magnitude of any residual stress assisting the creation of microcracks. The parameter λ will depend on the number of microcrack nuclei per unit volume, the ease with which they fail, the extent to which residual stress assists the failure, and the range of the magnitude of those residual stresses.

It should be noted that in general the distribution of microcracks generated by an applied stress is likely to be anisotropic in contrast to our assumptions. However, if residual stresses are important in the process of microcracking and those residual stresses are large, then the anisotropy will be limited and an isotropic model can be justified as a first approximation. The linearity of the microcrack density with applied stress can be viewed as reflecting a distribution of microcrack nuclei strengths, as arising from somewhat random distributions of residual stress on potential microcrack sites, or as a result of both. In any case, the mechanistic model for hypothetical microcracking in alumina[22,23] has this linear feature. The use of σ_e as the effective stress controlling the process of microcracking is a somewhat arbitrary choice among many combinations of stress invariants that could enter an isotropic-microcracking law. However, the use of σ_e has the virtue that it comes somewhat close to the criteria found to be useful by Fu and Evans.[22,23] In addition, its use ensures that both hydrostatic and deviatoric stress states produce microcracks. As an additional benefit, the use of σ_e in Eqs. (1*a*) through (1*c*) leads to a multiaxial continuum constitutive law that is nonlinear but hyperelastic. That is, the material is one for which the strain energy density is a potential with respect to strain that generates the stress–strain law. This, in turn, means that the J integral[25] is path independent and can be used in the analysis of stationary cracks.

In summary, it is likely that if microcracking occurs in a material, it will proceed in a manner described imprecisely by Eqs. (1*a*) through (1*c*). That is, there may be anisotropy and nonlinearity, and the stress-controlling microcracking will probably differ from σ_e. However, the simplifying features introduced in Eqs. (1*a*) through (1*c*) allow us to use an elementary theoretical model nevertheless containing basic elements of behavior thought to be relevant in a microcracking material.

It seems to be appropriate to use an upper limit for the microcrack density in materials like ZTA. In that case, the microcracks are observed at zirconia particles, and there are either one or no microcracks per particle.[2] Thus, the number of particles per unit volume and the maximum microcrack length (three alumina grain sizes in the case observed[2]) set this upper limit. In practice, the actual saturation density may be less than the upper limit. However, there are no other data supporting whether a saturation microcrack density is an appropriate assumption for other materials. For example, if grain-boundary microcracking is assumed to occur in alumina, there seems to be no reason why the process should terminate at some finite strain. Instead, as the strain is increased, we would expect grain boundaries to fail progressively as the load is shed onto the remaining intact grain interfaces. This would entail a progressive decrease in the stress-bearing capacity of the material until failure occurs. This behavior would lead to a nonlinear failure process around the macroscopic crack tip which would be described by a crack-tip singularity in macroscopic stress differing from the usual $r^{-1/2}$ form. We did not pursue this possibility but instead used the saturation limit on microcrack density at a level which ensures a finite elastic stiffness for macroscopic elements of the material. This concept of microcrack saturation was used also by Evans and Fu[15] and as in that paper gives rise to a zone of material of saturated microcrack density completely surrounding the macroscopic crack tip. The macroscopic stress field in this zone will have the usual $r^{-1/2}$ singularity characterized by a crack-tip stress-intensity factor.[15] A critical crack-propagation value of this factor and the associated fracture energy can be thought of as characterizing a very-small-scale near-tip failure-process zone in which the coalescence of the microcracks with each other and with the macroscopic crack takes place.

When considering the macroscopic stiffness of an element of microcracked material, we found that we can approximate the results of Budiansky and O'Connell[24] as

$$\overline{E}/E = \overline{\nu}/\nu = 1 - 16\epsilon/9 = 1/f \tag{2}$$

where E and $\overline{E}$ are Young's moduli and ν and $\overline{\nu}$ are Poisson's ratios for the unmicrocracked and microcracked materials, respectively. The auxiliary microcrack-density parameter, f, has been introduced and is defined in terms of ϵ by Eq. (2). Note that $\overline{E}$ and $\overline{\nu}$ are defined at a specified fixed value of ϵ. Thus, the multi-axial constitutive model for the microcracking solid becomes

$$e_{ij} = \frac{f + \nu}{E}\sigma_{ij} - \frac{\nu}{E}\sigma_{kk}\delta_{ij} \tag{3}$$

where $\mathbf{e}$ is the macroscopic strain, $\boldsymbol{\sigma}$ is the macroscopic stress, δ_{ij} is the Kronecker delta, and f obeys Eqs. (1) and (2). The constitutive Eq. (3) is valid only for values of the microcracking parameter, f, within the interval $0 \leq \epsilon < 9/16$.

In a state of uniaxial stress specified by σ, the material response is linear to a stress of σ_c. As shown in Fig. 1, microcracking commencing then causes nonlinearity in the stress–strain curve. After the stress reaches σ_m, linearity resumes with a lower modulus than the initial one. If the stress σ is reduced at any stage, the material will unload linearly on a line in the stress–strain diagram passing through the origin. Thus, there is no residual strain at macroscopic stress in this model. Consequently, the residual strain caused by relief by microcracks of tensile residual stress has been omitted in the present paper, and the effect only of modulus change caused by microcracking is taken into account.

III. Formulation of the Crack-Tip Problem

The high stresses near the tip of a long crack will cause microcracking in the near-tip region in the material of interest to us, as shown in Fig. 2. We will restrict our attention to the situation in which the zone of microcrack damage is very small compared to the body containing the crack as in Fig. 3. We will refer to this situation as small-scale microcracking. In this case, the microcrack zone will lie within a region of uncracked material. Some distance outside the zone, the stresses will be almost the same as when the material does not microcrack. When small-scale microcracking prevails, these stresses will be the singular, linear elastic crack-tip

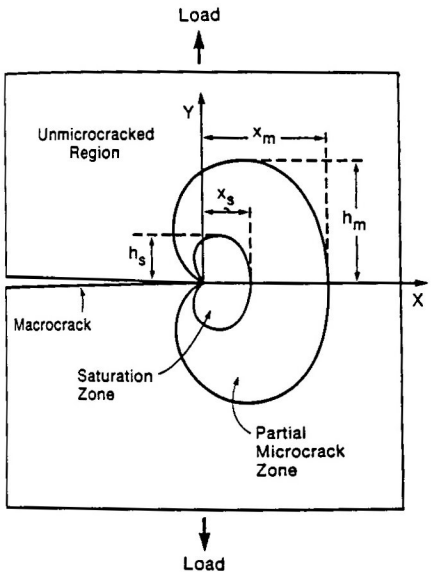

Fig. 2. Microcrack zone at a crack tip in a loaded body.

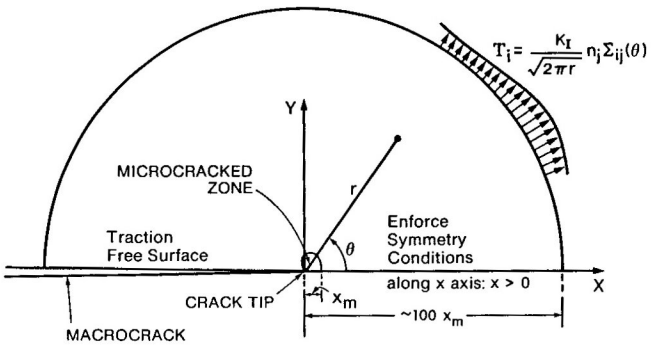

Fig. 3. Boundary conditions used in solving the finite-element equations for the small-scale-microcracking boundary-value problem.

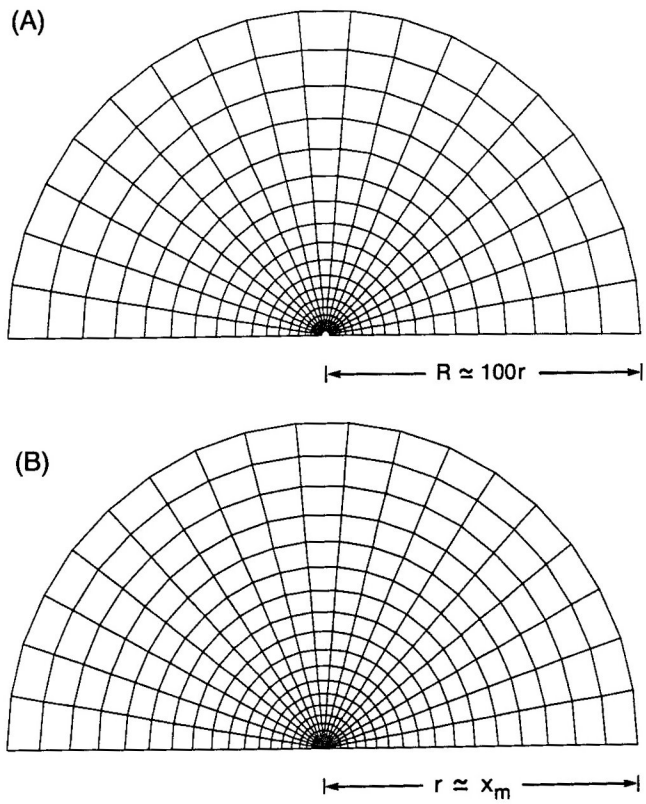

Fig. 4. (*A*) Finite-element mesh used in the finite-element analysis; (*B*) mesh which fits into the space at the center of mesh in (*A*).

stresses characterized by the stress-intensity factor K_I computed from the applied loads.

It follows that the plane-strain small-scale-microcracking problem can be solved by considering a plane region around the crack tip to which are applied boundary tractions given by the linear elastic stress field, i.e.

$$T_i = \eta_j \sigma_{ij} = \frac{K_I}{\sqrt{2\pi r}} \eta_j \Sigma_{ij}(\theta) \tag{4}$$

where T is the boundary traction, $\boldsymbol{\eta}$ is the outward unit normal to the region boundary, K_I is the mode I (tensile-opening mode) stress-intensity factor computed from the applied load, and (r,θ) are polar coordinates originating at the crack tip as shown in Fig. 3. The function $\boldsymbol{\Sigma}$ determines the angular distribution of stress, and its form can be found in the article by Rice.[26] The crack surfaces are traction free. To ensure small-scale microcracking, K_I must be limited to a sufficiently low level so that the zone size, X_m, as in Fig. 3 is small compared to the region for which the analysis is performed.

The governing equations of equilibrium and compatibility are enforced through the principle of virtual work

$$\int_A \sigma_{ij}\, \delta e_{ij}\, dA = \int_{S_T} T_i \delta u_i\, dS \tag{5}$$

in the absence of body forces, where A is the plane area being analyzed with S as its boundary, S_T is part of the perimeter where tractions are prescribed, $\mathbf{u}$ is the displacement, δ indicates a virtual variation of the quantity following it, and the variation disappears on $S - S_T$.

For plane-strain problems the constitutive law, Eq. (3), can be written as

$$\sigma_{\alpha\beta} = \frac{E}{f+\nu}\left(e_{\alpha\beta} + \frac{\nu}{f-2\nu} e_{\gamma\gamma}\delta_{\alpha\beta}\right) \qquad (\alpha,\beta,\gamma = 1,2) \tag{6a}$$

$$\sigma_{zz} = \nu\sigma_{\gamma\gamma}/f \tag{6b}$$

with f determined according to Eqs. (1) and (2) as before.

IV. Finite-Element Equations

The boundary-value problem specified in Section III must be solved by a numerical technique. A displacement-based finite-element method[27] was used for this purpose. The finite-element equations can be derived from the principle of virtual work given by Eq. (5). Finite-element interpolations for displacements, together with Eq. (5) and the constitutive law given by Eq. (6), give rise to the nonlinear finite-element equations

$$[\mathbf{K}(\mathbf{u}_n)]\{\mathbf{u}_n\} = \{\mathbf{F}_n\} \tag{7}$$

where $[\mathbf{K}]$ is the stiffness matrix, $\{\mathbf{u}_n\}$ is the nodal-displacement vector, and $\{\mathbf{F}_n\}$ is the force vector. The notation $[\mathbf{K}(\mathbf{u}_n)]$ indicates the dependence of the stiffness on the nodal displacements due to the nonlinear constitutive law.

In the finite-element analysis, 4-noded isoparametric quadrilateral elements with four stations for the integration of the stiffness were used. The finite-element mesh is shown in Fig. 4. The outer radius of the mesh is chosen to be ≈100 times the microcrack zone size (X_m) developed in the calculations. An iterative method is used to solve the finite-element equations. An initial estimate of the nodal displacements associated with the solution for the non-microcracking material is used to commence the iteration proce-

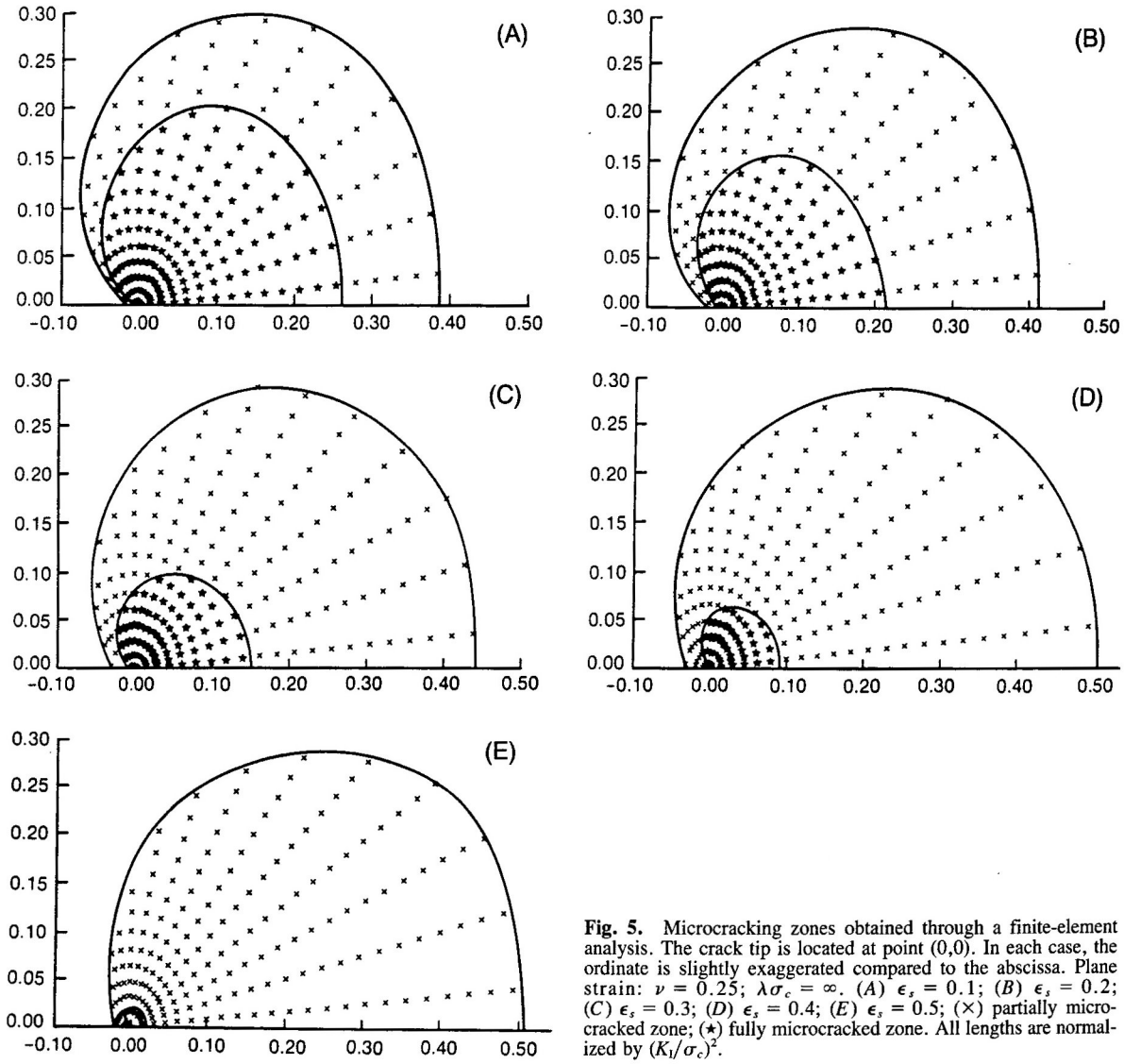

Fig. 5. Microcracking zones obtained through a finite-element analysis. The crack tip is located at point (0,0). In each case, the ordinate is slightly exaggerated compared to the abscissa. Plane strain: $\nu = 0.25$; $\lambda\sigma_c = \infty$. (*A*) $\epsilon_s = 0.1$; (*B*) $\epsilon_s = 0.2$; (*C*) $\epsilon_s = 0.3$; (*D*) $\epsilon_s = 0.4$; (*E*) $\epsilon_s = 0.5$; (×) partially microcracked zone; (★) fully microcracked zone. All lengths are normalized by $(K_I/\sigma_c)^2$.

dure. The strains at the integration stations are computed using standard-element interpolations, and the stress must be computed from those strain values. For this to be possible, the value of f must be computed first in terms of the strain. When Eq. (6) is used to compute σ_e and the result is substituted into Eq. (1*b*) with ϵ written in terms of f, a sixth-order polynomial equation in terms of f results. The coefficients of the polynomial are composed of the strain invariants and the material parameters σ_c, λ, E, and ν. Thus, the value of f can be obtained in terms of the strain and the material constants as the root of the polynomial equation. At most, one root of the polynomial equation lies within the admissible range for f. If the values for f all fall below unity or are imaginary, the material is unmicrocracked and $f = 1$. If f is so large that $\epsilon > \epsilon_s$, then $\epsilon = \epsilon_s$ and $1/f = 1 - 16\epsilon_s/9$. Once the value of f is established at each integration station, the stiffness matrix in Eq. (7) can be established.

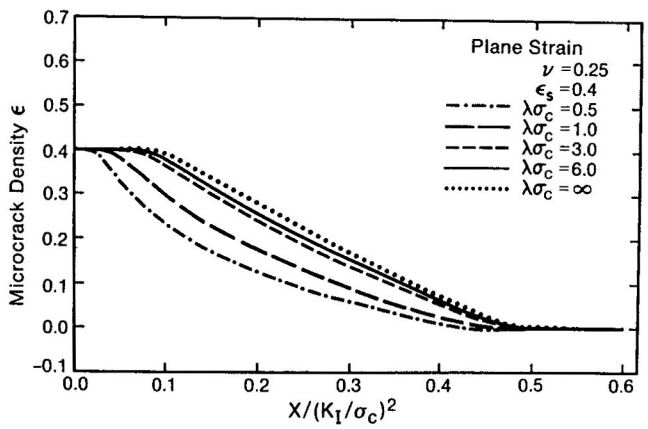

Fig. 6. Profile of the microcrack density ahead of the crack tip for $\epsilon_s = 0.4$ and various values of $\lambda\sigma_c$.

A secant method of iteration is used to determine the iterative improvements to Eq. (7) in terms of the nodal displacements. A convergence test on the mean square of the nodal displacements was used. This iterative method can be implemented because the model of microcracking used is a nonlinear hyperelastic material as long as no unloading occurs. This will be the case in the calculations for stationary cracks performed for this research.

V. Results

(1) *Shape and Size of the Microcracked Zone*

The regions of microcracking at the macrocrack tip are shown in Fig. 5 for different values of the saturation density. There is an inner region in which the microcrack density has reached the saturation level, ϵ_s. Between the fully microcracked material and the unmicrocracked outer field is a transition zone of partial microcracking. In no case does the inner zone become identical to the

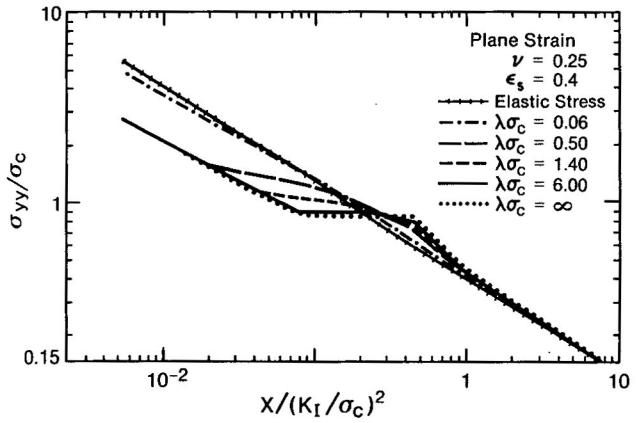

Fig. 7. Stress σ_{yy} ahead of the crack tip for $\epsilon_s = 0.4$ and various values of $\lambda\sigma_c$.

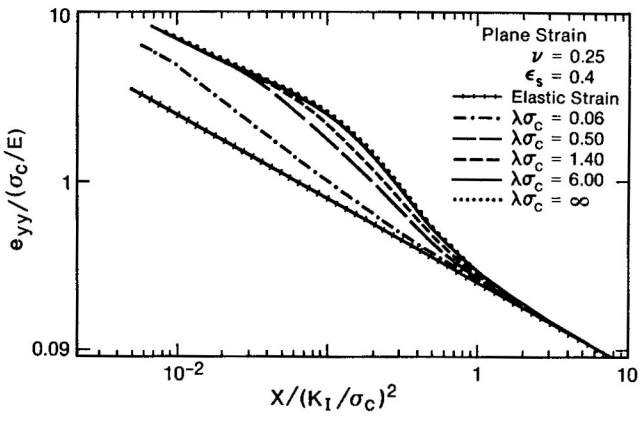

Fig. 8. Strain e_{yy} ahead of the crack tip for $\epsilon_s = 0.4$ and various values of $\lambda\sigma_c$.

outer zone because, as discussed below, gradual microcracking is an essential feature of the microcracking law of Eqs. (1) and (3). The height (transverse to the macrocrack), scaled by $(K_I/\sigma_c)^2$, is quite insensitive to the saturation density, whereas the breadth (parallel to the macrocrack), scaled in the same way, increases slightly with ϵ_s. The size and shape of the outer zone change little when different values of the product $\lambda\sigma_c$ are used. The relative insensitivity of the outer perimeter of microcracking to parameters other than K_I and σ_c reflects the fact that the initiation of microcracking is controlled by the stress levels generated by the magnitude of K_I and by the threshold stress, σ_c.

On the other hand, the size of the inner, saturated zone, depends not just on K_I and σ_c but also on ϵ_s as can be seen in Fig. 5. Furthermore, varying the product $\lambda\sigma_c$ causes noticeable changes to the size of the inner zone, as can be deduced from Fig. 6, which shows the microcrack density ahead of the crack for $\epsilon_s = 0.4$. This effect arises because increasing $\lambda\sigma_c$ at fixed ϵ_s and σ_c causes a reduction in σ_m, thus broadening the saturation zone. The trend of microcrack density ahead of the crack for $\epsilon_s = 0.4$ is fairly typical, although for other values of ϵ_s the inner zone has a different relative size.

The plots of microcrack density in Fig. 6 show clearly that there is a gradual transition from unmicrocracked to fully microcracked conditions ahead of the crack tip. This occurs even when $\lambda\sigma_c = \infty$. In that case, the microcracking develops at a constant value of σ_e and, consequently, $\sigma_m = \sigma_c$. No abrupt transition from intact to completely microcracked conditions occurs because the microcracking develops gradually as strain accumulates. In this sense, the case $\lambda\sigma_c = \infty$ is akin to nonhardening behavior in plasticity theory in which the plastic strain increases while the stress stays constant. The difference is that, in the microcracking model, the stress starts to rise again after microcrack saturation is reached. It should be noted that, even when $\lambda\sigma_c = \infty$, the intermediate zone spreads over many finite elements, and so the smooth transition is accurately modeled rather than being an artifact of the numerical method.

(2) Stress and Strain Fields

Figures 7 and 8 display the stress σ_{yy} and strain e_{yy} ahead of the crack tip for $\epsilon_s = 0.4$ and various choices of $\lambda\sigma_c$. In the unmicrocracked region, both stress and strain agree quite closely with the solution obtained without any microcracking taking place. The strain and stress fields in the unmicrocracked region constrain the deformation due to microcracking in the damaged zone. This constraint, together with the weakening of the material in the microcracked zone, causes stress relaxation in the region of intermediate microcracking (Fig. 7), and appreciable strain increase is observed there because of the modulus reduction (Fig. 8). Very close to the crack tip, the microcracking density is saturated, and the stress and strain fields become singular again but with a lower stress-intensity factor which will be denoted K_{tip}. In the case of $\lambda\sigma_c = 0.06$, the saturated zone is too small to be accurately represented by the finite-element mesh. We note also that the zone of intermediate microcracking permits a smooth, gradual transition for both the strain and stress fields from the outer to the inner fields. The effective stress σ_e ahead of the crack behaves in a manner very similar to σ_{yy} and is consistent with the microcracking law given by Eq. (3) and shown in Fig. 1. In the particular case of $\lambda\sigma_c = \infty$, $\sigma_e = \sigma_c$ in the transition region as expected. As noted previously, the partially microcracked zone is like a perfectly plastic zone in this situation.

VI. Microcrack Toughening

(1) Frontal-Zone Toughening

We shall now consider the influence of microcracking on the toughness of the material. First, we shall investigate the condition under which crack growth will initiate. Immediately the question arises: What criterion for initiation is appropriate? Two possibilities come to mind: (1) the crack will propagate when the tip energy-release rate reaches the critical level for the unmicrocracked material or a level somewhat reduced to account for proximity and coalescence effects of the nearby microcracks;[13–16] (2) the appropriate criterion is that K_{tip} equals the fracture toughness and that the level will be the same as for the unmicrocracked material or will be reduced somewhat by damage effects as before. These two possibilities will be considered below to investigate the level of crack-tip shielding which results.

Prior to inititation of crack propagation, the frontal-microcracking zones enclosed by a contour of critical effective stress $\sigma_e = \sigma_c$ are shown in Fig. 5. In the saturated region near the tip the material responds linearly. We have also noted that the material obeying the constitutive law of Eqs. (1) to (3) is nonlinear hyperelastic. It follows that the J integral[25] is path independent throughout the material in both microcracked and unmicrocracked regions. It should be noted that assumed path independence of the J integral for a microcracking material model has been invoked on weaker grounds by others.[13,15,17] As a consequence of J path independence, the crack-tip energy-release rate for small-scale microcracking will have the same value as in the nonmicrocracking material at the same applied loads. That is, the microcracking process causes no shielding of the energy flux to the crack tip. As pointed out by Evans and Faber,[13] if a Griffith energy-release-rate criterion is relevant for crack growth, then the macroscopic flaw will begin to propagate at the same applied load or applied K_I level in both the nonmicrocracking and microcracking versions of a given material, assuming that the critical energy-release rate is the same in both. In that case, there will be no microcrack toughening as far as crack-growth initiation is concerned. Indeed, it is likely that microcracks would serve to reduce the critical energy-release rate for crack propagation because they can provide easy paths for growth.[13] In that case, the net effect of microcracks would be

embrittlement, compared to the nonmicrocracking version of the same material.

The criterion based on fracture toughness, a K criterion, provides somewhat different predictions. Since the J integral is path independent in our model for a microcracking material and because linear elastic behavior prevails in the unmicrocracked material and in the tip saturation zone, it follows from the Irwin relationship that[13]

$$\frac{1-\overline{\nu}_s^2}{\overline{E}_s}K_{tip}^2 = \frac{1-\nu^2}{E}K_I^2 \tag{8}$$

where $\overline{E}_s$ and $\overline{\nu}_s$ are the values of Young's modulus and Poisson's ratio, respectively, in the saturated microcrack zone. The tip value of the stress-intensity factor, K_{tip}, will be less than the applied value, K_I, because $\overline{E}_s < E$. That is, microcrack shielding of the stress intensity does occur. If the propagation criterion is that K_{tip} equals the fracture toughness of the nonmicrocracking material, then it will take a higher applied-stress-intensity factor to initiate crack propagation in the microcracking material than in the nonmicrocracking version of the same material. Thus, microcrack toughening will have occurred, and it could be substantial if the microcrack saturation density is high. However, the damaging effects of near-crack-tip microcracks mentioned previously probably will reduce the effective toughness of the microcracking material. It is entirely possible that this effect will negate the benefits to toughness arising from shielding. This conclusion was drawn by Evans and Faber[13] and Evans and Fu,[15] although there are no data and no theoretical models on which to base any conclusions concerning the crack-growth-initiation toughness of microcracking materials.

In summary, the energy-release-rate criterion predicts no toughening nor a net deleterious effect due to microcracking, and the fracture-toughness criterion predicts some net toughening but little or none when damaging effects of near-tip microcracks are significant. Since the materials of interest to us in the present paper are brittle, the energy-release-rate criterion is the one most likely to be relevant. Near-tip microcracks will probably reduce the critical value by a fraction about equal to the area fraction of microcracks absorbed by the advancing macroscopic crack front. However, the crack would be deflected somewhat to absorb these microcracks, and this would compensate slightly for the damaging effect.

(2) *Wake-Zone Toughening*

At some level of the stress-intensity factor, the crack will begin to propagate. If the material microcracks, a wake of them will be left near the surface of the grown crack. This wake of material can contribute to crack-tip-shielding effects, and, when other mechanisms of shielding such as stress-induced phase transformations are involved, effects due to a wake zone are known to be generally stronger than those due to a frontal zone of an ungrown crack.[29–31] No finite-element calculations for a growing crack were performed for the present paper. However, results for a grown crack can be estimated from the stationary crack solutions by assuming that the distribution of microcrack densities created ahead of a growing crack are the same as those for a stationary crack. Thus, the density of microcracks in the wake at a distance y from the crack surface would be the same as the maximum density at that distance y in the frontal zone computed for the present paper. The extent of the wake would depend on the amount of crack growth that occurred. For each wake-zone extent, a calculation of the shielding effect could be performed using the results of Hutchinson.[18] It would be expected that an increasing amount of shielding would occur as the crack grows, and this would give rise to an R curve of the type observed during transformation toughening.[31] However, it is interesting simply to compute the shielding due to a very long wake. This will predict the asymptotic toughening approached by the R curve as the crack grows. Although the effective toughness of these materials depends on the interaction of the loading system with the R curve, the asymptotic value of toughening gives an upper bound to the effect and predicts a limit to the potency of this theoretical mode of microcrack toughening.

The toughening for the very long wakes can be estimated from energy-balance considerations.[15] At this stage the process of crack growth will have developed into a steady state in which the strains in the wake are invariant in a coordinate system moving with the crack tip. If the crack advances by a distance da, a strip of microcracked material of width da is effectively added in the wake remote from the tip without any alteration of the state of the wake close to the crack tip. All material points in this added strip are stress free, but a certain amount of energy is dissipated in creating the microcracks in this slice. The dissipated energy is dictated by the hysteresis energy shown in Fig. 1. The energy required to cause an increment of crack growth is the current crack-energy-release rate plus the energy stored or dissipated in creating the corresponding extra portion of the wake.[14,15] Therefore, the asymptotic fracture energy, G_w, is given by

$$G_w = G_c + 2\int_0^h H(y)\,dy \tag{9}$$

where G_c is the crack-energy-release rate at which the crack growth initiates. The latter parameter is evaluated in terms of the applied loads by the Irwin relationship

$$G_c = \frac{1-\nu^2}{E}K_c^2 \tag{10}$$

where K_c is the stress-intensity factor computed from the applied loads when the crack propagation commences. Consequently, G_c is the effective or apparent value rather than the actual crack-tip value of the energy release rate. The difference between the tip value and G_c is taken into account by any shielding or damage effect associated with microcracking around the stationary crack as previously discussed. Thus, there is no attempt here to tie G_w to some fundamental value of fracture energy; only the effective, apparent value at crack-growth initiation is related to G_w.

In Eq. (9), h is the height of the wake zone on one side of the crack, and H is the hysteresis energy as a function of y through the microcrack density $\epsilon(y)$. The hysteresis energy is the energy lost in a strain cycle from zero in the uncracked state, to the strain required to produce the specified microcrack density ϵ, and then linearly back to zero strain with the microcrack density fixed. As noted previously, the distribution $\epsilon(y)$ is determined from the microcracking results for a stationary, ungrown crack.

Since small-scale microcracking still prevails even after a long wake of microcracks are created, Eq. (9) can be rewritten in terms of the applied-stress-intensity factors

$$K_w^2 = K_c^2 + \frac{2E}{1-\nu^2}\int_0^h H(y)\,dy \tag{11}$$

where K_w is the applied-stress-intensity factor corresponding to steady-state crack propagation at the asymptotic level of toughness. The integrations in Eq. (11) were performed using the results of the finite-element calculations for microcracking around stationary cracks. The details are omitted.

(3) *Trends in Toughness for Steady-State Crack Growth*

In Fig. 9, resulting normalized toughening values K_w/K_c versus saturation microcrack density, ϵ_s, are plotted, for various values of $\lambda\sigma_c$. It should be noted that the results for K_w/K_c are independent of the size of the wake zones generated, as noted by Hutchinson.[18] Given that the toughening is independent of zone size, the remaining variables that can influence the ratio are $\lambda\sigma_c$ and ϵ_s. It can be seen that K_w/K_c goes to 0 as ϵ_s goes to 0. However, the toughening effect becomes substantial as ϵ_s approaches 9/16, the limit at which elastic moduli go to 0 in the Budiansky and O'Connell[24] model. Large toughening ratios are achieved when $\epsilon_s = 0.5$. The trend is clearly to higher levels and toward ∞ as $\epsilon_s \to 9/16$, but interpretation of this should be done with care. It is likely that the Budiansky and O'Connell model is inaccurate as $\epsilon_s \to 9/16$ because interactions between nearest-neighbor microcracks then would become important. More important is the consequence of the model used in the present paper for the generation of microcracks in which increases in microcrack density can only occur

because of increases in stress magnitude. Thus, the uniaxial stress–strain curve for continuous increase of strain will be monotonic, and $\epsilon_s \to 9/16$ implies that the curve will flatten as microcrack densities rise. This will cause the hysteresis energy for a full cycle of stressing to approach infinity as $\epsilon_s \to 9/16$. The trend of toughening as $\epsilon_s \to 9/16$ shown in Fig. 9 can be understood in these terms.

The toughening ratio increases with $\lambda\sigma_c$ when ϵ_s is held fixed, as can be seen in Fig. 9. This arises because the hysteresis energy per unit volume increases with $\lambda\sigma_c$ if σ_c is fixed. Since σ_c plays no direct role alone in determining the contribution to toughness (it determines the wake-zone height which does not affect K_w/K_c), the result is that the toughening ratio increases with $\lambda\sigma_c$.

(4) Comparison with Other Models

Shielding effects due to hypothetical microcracking in wake zones around propagated cracks were estimated from a theoretical model by Evans *et al.*[13–15] and Hutchinson.[18] In those models, both the effect of modulus reduction and dilatation due to microcracking are taken into account, but their results only for the modulus effect will be compared with our solutions. The results of Evans *et al.*[13–15] indicate that the toughening ratio due to the modulus effect diminishes with $\lambda\sigma_c$. This contrasts to our results in which the ratio K_w/K_c increases with $\lambda\sigma_c$. However, it should be noted that both sets of results are approximate. Those of Evans *et al.*[13–15] are based on some assumptions about microcrack distributions, and ours are obtained with microcrack distributions determined for a stationary, ungrown crack.

Hutchinson[18] computed the shielding effect of microcracks to the lowest order in ϵ by using a perturbation approach to the elasticity problem. Along with other criteria, he used the same microcracking law that we used, with $\lambda\sigma_c = \infty$. He gave results for both stationary, ungrown cracks and for cracks with a long, microcracked wake. Using these two calculations together, one can determine that his predictions for the toughening ratio is

$$K_w/K_c = 1 + 0.31\epsilon_s \tag{12}$$

This was plotted in Fig. 9, and it can be seen that there is reasonably good agreement for $\epsilon_s < 0.3$. The results of Hutchinson[18] deviate from ours at higher value of ϵ_s because his method cannot account for the large differences in modulus then introduced. In addition, it should be remembered that our calculations are also approximate.

(5) Estimate for ZTA

Rühle *et al.*[2] estimated the modulus of the microcracked material near the crack surface in ZTA in which the zirconia is mostly monoclinic before the crack growth experiment was performed. They estimated a lowest value, ≈30% of the modulus of the uncracked material. This corresponds to a saturation density for round microcracks with $\epsilon_s \approx 0.4$. Then using the result for $\lambda\sigma_c = \infty$ in Fig. 9 as providing the lowest bound, we predict $K_w/K_c \approx 1.2$ because of the modulus effect alone on toughness. This neglects any contribution from dilatancy arising from the microcracks, which Rühle *et al.*[2] indicate is significant. Note also that K_w is an asymptotic value which will never be reached because of compliance of the loading system and the fracture specimen. On the other hand, the result for $\lambda\sigma_c = \infty$ is a lower bound to K_w/K_c and finite values for this parameter give larger toughening ratios. A finite value of $\lambda\sigma_c$ is likely to be appropriate to ZTA.

The toughness of the ZTA for which microcracking is observed is 6 MPa·m$^{1/2}$.[1] Using this as K_w, we deduce that the contribution to the toughness due to the modulus-reduction effect of microcracking could be 1 MPa·m$^{1/2}$. This is insufficient to explain the toughness of the ZTA since alumina has a toughness of ≈2.5 MPa·m$^{1/2}$. However, the result does indicate that this source of toughness could be significant in the ZTA involved.

VII. Conclusion

The theoretical model used in the present paper is by no means exact, but it contains features one would expect to govern microcracking and the associated toughening. The magnitudes of the parameters used are based on observation or are chosen to provide lower bounds on the toughness increment. Thus, the estimate of the toughening contribution due to modulus-reduction effects of microcracking is deemed reasonable for the ZTA involved. Clearly, other extrinsic sources of toughness also are operating in this material.

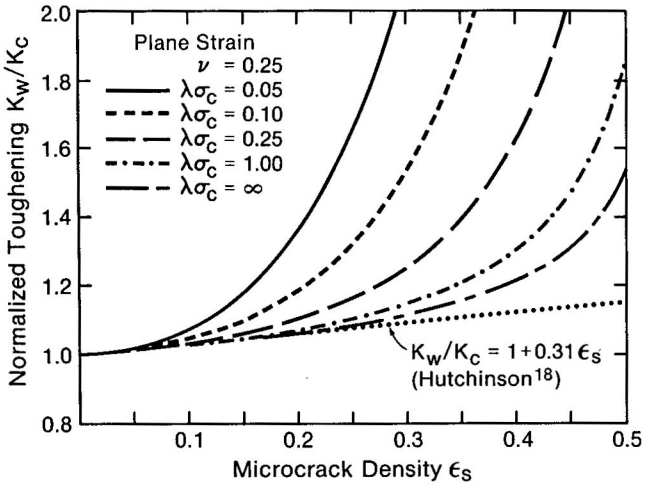

Fig. 9. Asymptotic toughening, K_w, versus the saturation microcrack dentisy, ϵ_s, for cracks with long microcrack wakes for various values of $\lambda\sigma_c$.

Acknowledgment: We acknowledge many helpful discussions with A. G. Evans.

References

[1]M. Rühle, N. Claussen, and A. H. Heuer, "Transformation and Microcrack Toughening as Complementary Processes in ZrO_2-Toughened Al_2O_3," *J. Am. Ceram. Soc.*, **69** [3] 195–97 (1986).
[2]M. Rühle, A. G. Evans, R. M. McMeeking, P. G. Charalambides, and J. W. Hutchinson, "Microcrack Toughening in Alumina/Zirconia," *Acta Metall.*, **35** [11] 2701–10 (1987).
[3]M. Friedman, J. Handin, and G. Alani, "Fracture-Surface Energy of Rocks," *Int. J. Rock Mech. Min. Sci.*, **9**, 757–66 (1972).
[4]R. G. Hoagland, G. T. Hahn, and A. R. Rosenfield, "Influence of Microstructure on Fracture Propagation in Rock," *Rock Mech.*, **5**, 77–106 (1973).
[5]A. G. Evans and M. Linzer, "Failure Prediction in Structural Ceramics Using Acoustic Emission," *J. Am. Ceram. Soc.*, **56** [11] 575–81 (1973).
[6]R. G. Hoagland, C. W. Marshall, A. R. Rosenfield, G. Hollenberg, and R. Ruh, "Microstructural Factors Influencing Fracture Toughness of Hafnium Titanate," *Mater. Sci. Eng.*, **15**, 51–62 (1974).
[7]H. Hübner and W. Jillek, "Subcritical Crack Extension and Crack Resistance in Polycrystalline Alumina," *J. Mater. Sci.*, **12**, 117–25 (1977).
[8]R. Knehans and R. Steinbrech, "Memory Effects of Crack Resistance During Slow Crack Growth in Notched Al_2O_3 Bend Specimens," *J. Mater. Sci. Lett.*, **1**, 327–29 (1982).
[9]P. L. Swanson, C. J. Fairbanks, B. R. Lawn, Y-W. Mai, and B. J. Hockey, "Crack-Interface Grain Bridging as a Fracture-Resistance Mechanism in Ceramics: I, Experimental Study on Alumina," *J. Am. Ceram. Soc.*, **70** [4] 279–89 (1987).
[10]R. G. Hoagland, J. D. Embury, and D. J. Green, "On the Density of Microcracks Formed During the Fracture of Ceramics," *Scr. Metall.*, **9**, 907–909 (1975).
[11]A. G. Evans, "On the Formation of a Crack Tip Microcrack Zone," *Scr. Metall.*, **10**, 93–97 (1976).
[12]R. G. Hoagland and J. D. Embury, "A Treatment of Inelastic Deformation Around a Crack Tip due to Microcracking," *J. Am. Ceram Soc.*, **63** [7–8] 404–10 (1980).
[13]A. G. Evans and K. T. Faber. "Toughening of Ceramics by Circumferential Microcracking," *J. Am. Ceram. Soc.*, **64** [7] 394–98 (1981).
[14]A. G. Evans and K. T. Faber, "Crack-Growth Resistance of Microcracking Brittle Materials," *J. Am. Ceram. Soc.*, **67** [4] 255–60 (1984).
[15]A. G. Evans and Y. Fu, "Some Effects of Microcracks on the Mechanical Properties of Brittle Solids: II, Microcrack Toughening," *Acta Metall.*, **33**, 1525–31 (1985).
[16]M. Kachanov, "Interaction of a Crack with Certain Microcrack Arrays"; unpublished work.
[17]M. Ortiz, "A Continuum Theory of Crack Shielding in Ceramics," *J. Appl. Mech.*, **54**, 54–58 (1987).
[18]J. W. Hutchinson, "Crack-Tip Shielding by Microcracking in Brittle Solids," Rept. No. MECH-87, Division of Applied Sciences, Harvard University, Cambridge, MA, 1986.
[19]L. M. Kachanov, Introduction to Continuum Damage Mechanics. Martinus Nijhoff, Netherlands, 1986.
[20]D. Krajcinovic and G. U. Fonseka, "The Continuous Damage Theory of Brittle Materials — Parts I and II," *J. Appl. Mech.*, **48**, 809–24 (1981).

[21]D. Krajcinovic, "Continuous Damage Mechanics Revisited: Basic Concepts and Definitions," *J. Appl. Mech*, **52**, 829–34 (1985).
[22]Y. Fu and A. G. Evans, "Microcrack Zone Formation in Single-Phase Polycrystals," *Acta Metall.*, **30**, 1619–25 (1982).
[23]Y. Fu and A. G. Evans, "Some Effects of Microcracks on the Mechanical Properties of Brittle Solids: I, Stress–Strain Relations," *Acta Metall.*, **33**, 1515–23 (1985).
[24]B. Budiansky and R. J. O'Connell, "Elastic Moduli of a Cracked Solid," *Int. J. Solids Struct.*, **12**, 81–97 (1975).
[25]J. R. Rice, "A Path-Independent Integral and the Approximate Analysis of Strain Concentration by Cracks and Notches," *J. Appl. Mech.*, **35**, 379–86 (1968).
[26]J. R. Rice, "Mathematical Analysis in the Mechanics of Fracture"; pp. 192–308 in Fracture, An Advanced Treatise, Vol. 2. Edited by H. Liebowitz. Academic Press, New York, 1968.
[27]O. C. Zienkiewicz, The Finite Element Method, 3d ed. McGraw-Hill, New York, 1977.
[28]P. G. Charalambides, "Near-Tip Mechanics of Stress-Induced Microcracking in Brittle Materials," Ph.D. Dissertation. University of Illinois at Urbana-Champaign, 1986.
[29]R. M. McMeeking and A. G. Evans, "Mechanics of Transformation Toughening in Brittle Materials," *J. Am. Ceram. Soc.*, **65** [5] 242–46 (1982).
[30]B. Budiansky, J. W. Hutchinson, and J. C. Lambropoulos, "Continuum Theory of Dilatant Transformation Toughening in Ceramics," *Int. J. Solids Struct.*, **19**, 337–55 (1983).
[31]A. G. Evans and R. M. Cannon, "Toughening of Brittle Solids by Martensitic Transformations," *Acta Metall.*, **34**, 761–800 (1986). □

J. Am. Ceram. Soc., **71** [6] 472–77 (1988)

Accumulation of Creep Damage in a Siliconized Silicon Carbide

DANIEL F. CARROLL* and RICHARD E. TRESSLER*

Department of Materials Science and Engineering, The Pennsylvania State University, University Park, Pennsylvania 16802

The accumulation of creep damage in a siliconized silicon carbide was investigated as a function of applied stress, creep strain, and microstructure. At 1100°C, creep damage was observed to accompany deformation in specimens tested to creep strains greater than 0.10%, under applied stresses greater than 137 MPa. At low creep strains, creep damage occurred in regions of the microstructure of high silicon carbide content. As deformation progressed, creep damage extended into regions of the microstructure of lower silicon carbide content. The area density and area fraction of cavities were found to increase linearly with creep strain. From these results, a threshold stress for the formation of creep damage was determined to be 132 MPa at 1100°C. It was suggested that the formation of creep damage was controlled by the heterogeneous nucleation of cavities at the silicon–silicon carbide interface, with the aid of high localized stresses and iron impurities in the silicon phase.

Manuscript No. 199921. Received July 15, 1987; approved December 9, 1987.
Presented at the 89th Annual Meeting of the American Ceramic Society, Pittsburgh, PA, April 28, 1987 (Basic Science Division, Paper No. 143–B–87).
Supported in part by the U.S. Army Research Office, Metallurgy and Materials Science Division.
*Member, the American Ceramic Society.

I. Introduction

SILICON CARBIDE based ceramics are currently being considered for high-temperature structural applications due to their good mechanical strength and oxidation resistance at elevated temperatures.[1,2] One such material is siliconized silicon carbide. Siliconized silicon carbide is a two-phase material whose microstructure consists of interpenetrating phases of silicon and silicon carbide. The silicon phase is dispersed throughout the continuous silicon carbide phase in either a continuous or noncontinuous matrix, depending upon the amount of free silicon in the material.

Past investigations have shown that cavity formation or creep damage occurs in some types of siliconized carbides under load at elevated temperatures.[3–5] In these bend tests, the creep damage was confined to the tensile side of the bend beams and increased with deformation. Carroll and Tressler[3] have shown that this creep damage can result in strength degradation at room temperature. Wiederhorn *et al.*[4] have shown that creep damage can also lead to strength degradation and failure at elevated temperatures. Since strength degradation and delayed failure can occur in siliconized silicon carbide, the accumulation of creep damage must be understood as a function of deformation, before these materials can be used in high-temperature structural applications.

Typically, deformation studies are conducted in bending. However, stress redistribution may occur in a bend beam during deformation. Stress redistribution is possible when a material exhibits